

# RSC Advances



This is an *Accepted Manuscript*, which has been through the Royal Society of Chemistry peer review process and has been accepted for publication.

*Accepted Manuscripts* are published online shortly after acceptance, before technical editing, formatting and proof reading. Using this free service, authors can make their results available to the community, in citable form, before we publish the edited article. This *Accepted Manuscript* will be replaced by the edited, formatted and paginated article as soon as this is available.

You can find more information about *Accepted Manuscripts* in the [Information for Authors](#).

Please note that technical editing may introduce minor changes to the text and/or graphics, which may alter content. The journal's standard [Terms & Conditions](#) and the [Ethical guidelines](#) still apply. In no event shall the Royal Society of Chemistry be held responsible for any errors or omissions in this *Accepted Manuscript* or any consequences arising from the use of any information it contains.

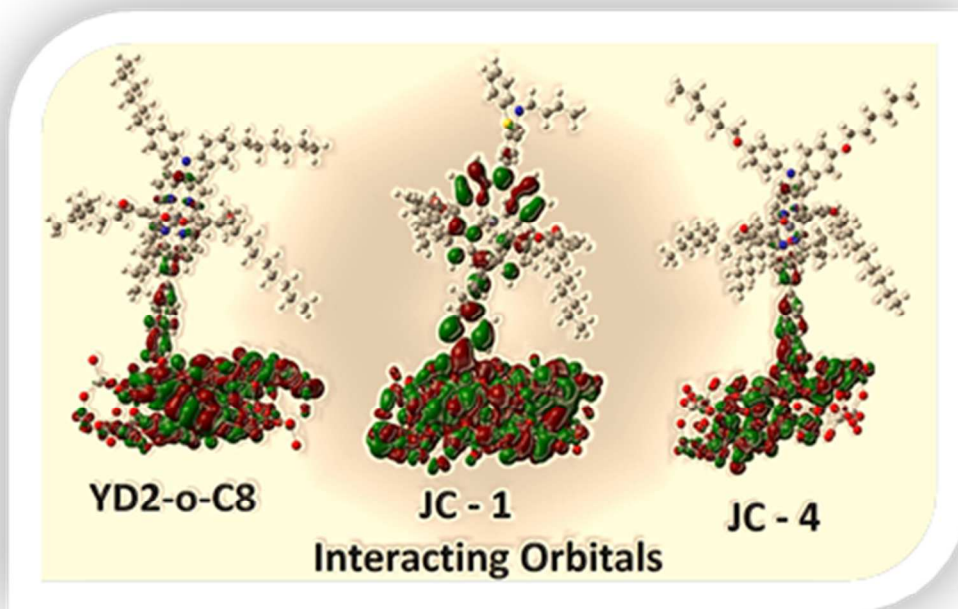
## GRAPHICAL ABSTRACT

AUTHOR NAMES: Kadali Chaitanya, Xue-Hai Ju, and B. Mark Heron

TITLE: Theoretical Study on the Light Harvesting Efficiency of Zinc Porphyrin Sensitizers for DSSCs.

TEXT: DFT and TDDFT calculations have been carried out to investigate the effect of donor and acceptor groups on the electronic properties of zinc-porphyrin sensitizers. The calculated results show that increasing the electron releasing strength of a *meso*-donor group opposite to a *meso* substituted acceptor group increases the light harvesting efficiency and short circuit current density.

GRAPHICAL ABSTRACT FIGURE



## Theoretical Study on the Light Harvesting Efficiency of Zinc Porphyrin Sensitizers for DSSCs

Kadali Chaitanya<sup>1</sup>, Xue-Hai Ju<sup>\*1</sup>, and B. Mark Heron<sup>2</sup><sup>1</sup> Key Laboratory of Soft Chemistry and Functional Materials of MOE, School of Chemical Engineering, Nanjing University of Science and Technology, Nanjing, P. R. China, 210094<sup>2</sup> Department of Chemical and Biological Sciences, School of Applied Sciences, University of Huddersfield, Queensgate, Huddersfield, HD1 3DH, UK.**ABSTRACT**

The density functional theory and time-dependent density functional theory calculations of the electronic structures and electronic absorption spectra of a series of zinc porphyrin based sensitizers were reported. The sensitizers comprise of either 10*H*-phenothiazin-3-yl or bis(4-(hexyloxy)phenyl)amino and acene bridged carboxylic acid as an electron donating and accepting units, respectively. The dye/(TiO<sub>2</sub>)<sub>36</sub> anatase nanoparticle systems were also simulated to show the electronic structure on the interface. The calculated results show that a strong electron-donating capacity of the donor group attached at the *meso*-position opposite to the anchoring group of the dye will increase the molecular extinction coefficient, excited state lifetime, light harvesting efficiency and decrease the reorganization energy as compared to the structurally similar reference dye *YD2-o-C8*. The calculated short circuit current density and level alignment quality clearly indicate that the zinc-porphyrin dyes substituted with 10*H*-phenothiazin-3-yl donor and either 4-ethynylbenzoic acid or 4-ethynyl-1-naphthoic acid offer potential for use in DSSCs due to their large values when compared to the reference dye. The results obtained in this study will certainly provide a useful reference to the future design of tetra-substituted zinc porphyrins for dye sensitized solar cell applications.

**Keywords:** Zinc Porphyrin, Phenothiazine, Dye-sensitized solar cell, TDDFT, Electronic structure.

**1. INTRODUCTION**

Over the last two decades there has been sustained effort directed towards the replacement Si-containing solar cells [1] with dye-sensitized solar cells (DSSCs) containing either organometallic or fully organic photosensitizers for a variety of reasons including environmental issues, lower cost, and the possibility to obtain very high extinction coefficients leading to greater efficiencies [2-5]. Recently, various dye classes, such as perylene dyes [6], cyanine dyes [7], merocyanine dyes [8], coumarin dyes [9], porphyrin dyes [10], and indoline dyes [11], have been investigated as sensitizers yielding respectable conversion efficiencies between 5 and 12% with the traditional iodide/triiodide redox system. Several review articles have summarized the properties of these new sensitizers [12-14]. Amongst all of these dyes, porphyrin derivatives are considered as efficient sensitizers for DSSC applications because of their high extinction coefficients and exceptional photophysical properties and photochemical stability [15]. The efficiencies of porphyrin-

<sup>1</sup> Corresponding Author (Prof. Xue Hai Ju)

\*E-mail: xhju@njust.edu.cn

based DSSCs have increased steadily in recent years. For example, Yella and coworkers [16] showed that it is possible to obtain higher open-circuit voltages with one of the Zinc metalloporphyrin (Zn-porphyrin) complexes, the so called YD2-o-C8 dye (see figure 1), leading to power-conversion efficiency of 12% under simulated air mass (AM) 1.5 global sunlight.

In DSSCs, the sunlight-to-electricity conversion efficiency ( $\eta$ ) of solar cell devices is determined by the open-circuit photovoltage ( $V_{OC}$ ), short-circuit current density ( $J_{SC}$ ), and the fill factor (FF), as compared to incident solar power ( $P_{inc}$ )

$$\eta = \frac{(V_{OC}) (J_{SC}) (FF)}{P_{inc}} \quad (1)$$

According to Equation (1), the product of  $V_{OC}$  and  $J_{SC}$  should be optimized to improve the efficiency of  $\eta$ . However, further improvement in efficiency relies on a better understanding of the role of the dye in the energy conversion mechanisms and precise modeling for design optimization.

To predict the photophysical properties of the dye photosensitizer in a DSSC, it is essential to understand the sensitization of a wide band gap semiconductor, typically  $TiO_2$ , via electron injection from a photoexcited chromophore to ensure device stability [17]. The rate of charge transfer (CT) is governed by the free energy of the transition, which is related to the electronic potential energy levels [highest occupied molecular orbitals (HOMOs) and lowest unoccupied molecular orbitals (LUMOs)] of both the donors and the acceptors. The LUMOs of the Zn-porphyrin sensitizers are generally too low to provide perfect electron injection, and should be further increased by the use of optimizations. The characteristic electronic absorption spectrum of a porphyrin species consists of a strong transition to the second excited state ( $S_0 \rightarrow S_2$ ) at about 400 nm (the Soret or B band) and a weak transition to the first excited state ( $S_0 \rightarrow S_1$ ) at about 550 nm (the Q band). The B and the Q bands both arise from  $\pi-\pi^*$  transitions and can be explained by considering the Gouterman four orbital model. According to Gouterman's four-orbital model, the near-degeneracy of the HOMO  $\rightarrow$  LUMO and HOMO-1  $\rightarrow$  LUMO transitions causes strong configuration mixing. The transition dipoles of the two configurations add, resulting in the intense Soret band. In the relatively weak Q band the transition dipoles of the two configurations nearly cancel [18]. This causes insufficient light harvesting in the region 450–650 nm, which is another limit to the performance of the Zn-porphyrin sensitizers. Due to the foregoing features Zn-porphyrin sensitizers are considered only as near-infrared sensitizers [19].

Zn-porphyrin complexes would be much more promising for developing panchromatic sensitizers and, thus, provide much higher efficiencies, if new absorption bands could be created in the visible light region. It is anticipated that perturbing the potential energy levels of the Zn-porphyrin dye by changing substituents may induce a substantial effect on the efficiency of devices [20]. Several researchers have reported the tuning of the photophysical properties of a porphyrin by the judicious placement of either electron - donating or -withdrawing groups [21-30]. Another approach to improving the performance of the porphyrin dyes is to extend their  $\pi$ -system, which leads to broadening and red shifting of the absorption bands, thus enhancing their light-harvesting efficiency.

In addition to experimental investigations, computational calculations have also been used to interpret the structure–performance relationships and screen promising candidates of various sensitizers used in DSSCs [31-35]. However, for the design and screening of better molecules and materials in which large quantities of samples are required to be computed in a relatively short time, computation efficiency is much preferred to high accuracy and complex models. Recent work on Zn-porphyrin complexes have demonstrated that computational methods can be utilized to gain an understanding of the electronic properties of the complexes in solution [36]. A theoretical screening by Gratzel and co-workers [31] showed that preparing porphyrin sensitizers in a suitable donor-acceptor fashion might create a highly efficient porphyrin sensitizer. Several authors in their investigations showed that, with a reasonable computational effort, the density functional theory (DFT) and time dependent density functional theory (TD-DFT) successfully reproduced the experimentally observed spectroscopic and redox properties of the complexes [37, 38].

The photoconversion efficiencies of DSSCs fabricated using metalloporphyrin dye molecules deeply depend on the molecular structures (i.e., donor (D) and acceptor (A) groups of the dyes) and the amount of dye adsorbed on the TiO<sub>2</sub> surface. The tetrasubstituted Zn-porphyrin YD2-o-C8 was shown to be responsible for the excellent cell performance of a DSSC device [16]. The sensitizer YD2-o-C8 has one *meso*-position of the porphyrin core attached to a strong electron diphenylamine donor, the opposite *meso* position is substituted with a linker via an ethynyl bridge with a carboxylic acid group serving as the anchoring group for dye adsorption to the surface of TiO<sub>2</sub> [16]. To further improve the device performance, Reddy et al. [39] modified the phenyl bridge between the carboxyl and porphyrin ring in YD2-o-C8 with either naphthalene or anthracene units to increase  $\pi$ -extension, resulting in a slight red shift of both the Soret and Q bands compared to the YD2-o-C8. Therefore a high photovoltaic performance of a zinc porphyrin dye can be attained by attaching an anchoring group with a spacer, by incorporating a  $\pi$ -conjugated acene group to extend the light harvesting spectral range, by applying an electron donating group or by adding a polycyclic aromatic group to the  $\pi$ -conjugation system [40].

From the above discussion we knew that a suitable combination of acceptor, donor and  $\pi$ -bridge can effectively narrow the optical band gap of the molecule by maintaining a relatively low-lying E<sub>HOMO</sub> energy level, and consequently, an enhanced short-circuit current (J<sub>sc</sub>) and V<sub>oc</sub> value can be expected. Recently, Mathew *et al.*, modified the donor and acceptor units in YD2-o-C8 with bis(2',4'-bis(hexyloxy)-[1,1'-biphenyl]-4-yl)amine and benzothiadiazole units, leading to the so called sensitizers SM371 and SM315 which in a device exhibited a high open-circuit voltage V<sub>oc</sub> of 0.91 V, short-circuit current density J<sub>sc</sub> of 18.1 mA cm<sup>-2</sup>, fill factor of 0.78 and a power conversion efficiency of 13% [41]. Therefore, in the present study, we present the theoretical screening of zinc porphyrin dyes with either a 10*H*-phenothiazin-3-yl or a bis(4-(hexyloxy)phenyl)amino unit as an electron donating group instead of a diphenylamine unit in the reference dye YD2-o-C8 in order to obtain better light absorption properties in the UV–visible–near IR region. For this a C<sub>6</sub>H<sub>3</sub>(OC<sub>8</sub>H<sub>17</sub>)<sub>2</sub> ancillary ligand with either a naphthalene or an anthracene bridging moiety and a carboxylic acid as the anchoring group were substituted on a Zn-porphyrin core structure. Thus two interrelated series of substituted porphyrin dyes, which are variants of the established, dye YD2-o-C8, were postulated and evaluated. One series (JC1 – 3) examines

the replacement of the *meso* diphenylamine donor unit of YD2-o-C8 with the well-established phenothiazine electron donor unit. Here steric interactions between the *ortho* H-atoms of the propeller-shaped diphenylamine unit and the porphyrin ring H-atoms are minimised by use of a more planar, less hindered phenothiazine unit, which should result in changes in  $\lambda_{\text{max}}$  of the proposed dyes relative to YD2-o-C8, with an attendant change in photon capture. The second series (JC4 – JC6) retain the diphenylamine motif but vary the terminal donor units from hexyl *viz.* YD2-o-C8 to hexyloxy with the anticipation that a bathochromic shift in absorption maximum will be induced. Within each of the foregoing series the steric demand of the 4-ethenyl-1-benzoic acid anchoring group is increased through the fusion of extra phenyl rings to the benzoic acid unit to afford, sequentially, 4-ethenylnaphthalene-1-benzoic acid and thence 10-ethenylanthracene-9-carboxylic acid. The anchoring and alignment of the dye unit to the surface of the TiO<sub>2</sub> has proved important in the performance of DSSCs. Here increased steric interactions are probed by increasing the number of *peri* H atoms (naphthalene → anthracene) which may interfere with the binding of the carboxylic acid group with the TiO<sub>2</sub> surface. The electronic properties of the two series of dyes were studied using density functional theory and time-dependent density functional theory calculations. The molecular structures of zinc porphyrins JC1 to JC6 studied in this work are shown in Figure. 1. The results obtained in this study will certainly provide a useful reference to the future design and optimisation of tetra-substituted porphyrins for DSSC applications.

**Figure 1**

## 2. COMPUTATIONAL DETAILS

The molecular calculations were carried out with the Gaussian 03 code [42]. Geometry for all the Zn-porphyrin dyads has been fully optimized at DFT level. For geometry optimization the double- $\zeta$  quality basis set LanL2DZ [43] has been used throughout. This basis set contains the pseudopotentials for the metal atoms and has already proved efficient in the computation of Zn – porphyrin complexes properties [44]. UV/vis spectra have been calculated as vertical excitations from previously obtained ground state minimum (Franck–Condon principle) at the TD-DFT level with the CAM-B3LYP method [45]. The solvent effects of tetrahydrofuran were modelled using a conductor-like polarizable continuum model (C-PCM) within the self-consistent reaction field (SCRF) theory [46, 47]. The dye relaxation of the molecules was calculated using TD-B3LYP/LANL2DZ method. To understand the nature of electronic excitations, the excited states were analysed by constructing the frontier molecular orbitals (FMOs) within the Gaussian program package [42]. To gain insight into the electronic injection capability of dyes, the adsorption of dyes on the (TiO<sub>2</sub>)<sub>36</sub> cluster was investigated with DFT calculations using DMol<sup>3</sup> program in Material Studio Version 5.5 [48]. The (TiO<sub>2</sub>)<sub>36</sub> configuration was fully optimised using the generalized gradient-corrected approximation (GGA) method. The Perdew-Burke-Ernzerhof (PBE) functional was used to take into account of the exchange-correlation effects with DNP basis set. The core electron was treated with effective core pseudopotentials. After optimization, the adsorption energies ( $E_{\text{ads}}$ ) of dyes on the (TiO<sub>2</sub>)<sub>36</sub> cluster were obtained using the equation:

$$E_{\text{ads}} = E_{\text{dye+TiO}_2} - E_{\text{dye}} - E_{\text{TiO}_2} \quad (2)$$

Where  $E_{\text{dye}}$  was the total energy of isolated dye,  $E_{\text{TiO}_2}$  was total energy of  $(\text{TiO}_2)_{36}$  cluster, and  $E_{\text{dye+TiO}_2}$  was the total energy of dye -  $(\text{TiO}_2)_{36}$  complex. Following the above expression, a negative  $E_{\text{ads}}$  indicates that the molecule adsorption is exothermic and thus the adsorption system is energetically stable [49].

### 3. RESULTS AND DISCUSSION

#### 3.1. Proper choice of donor and acceptor groups

In order to enhance the light harvesting efficiency of DSSCs, the appropriate choice of donor and acceptor groups are essential. Generally, a strong electron donating group results a high  $E_{\text{HOMO}}$  energy level, whereas a strong electron accepting group will have a low  $E_{\text{LUMO}}$  energy level. Therefore we have calculated electron donating and accepting strengths of isolated molecules (**D1**: bis(4-hexylphenyl)amine; **D2**: bis(4-(hexyloxy)phenyl)amine; **D3**: 10*H*-phenothiazin-3-yl; **A1**: 4-ethynylbenzoic acid; **A2**: 4-ethynyl-1-naphthoic acid; and **A3**: 10-ethynylanthracene-9-carboxylic acid) attached to *meso*-position of the porphyrin  $\pi$ -bridge, which are in the following order: **D2** > **D3** > **D1** and **A3** < **A2** < **A1** (See Table 1). The electron donating and accepting strength of the donor and acceptor groups determine the  $E_{\text{HOMO}}$  and  $E_{\text{LUMO}}$  energy levels of a sensitizer, which are directly related to the charge transfer kinetics at the  $\text{TiO}_2$ /dye/electrolyte interface such as dye regeneration and recombination process [28]. To attain a high efficiency of the excited state electron injection, the  $E_{\text{LUMO}}$  energy level of the electron donor is usually required to be higher than that of the electron acceptor (at least 0.3 eV) in order to have sufficient driving force for electron transfer from the donor to acceptor. From the Table 1, we can see that the  $E_{\text{LUMO}}$  energies of the donors **D1** – **3** are in the range -0.406 to -0.691 eV, whereas  $E_{\text{LUMO}}$  energies of acceptors **A1** – **3** are in the range -1.868 to -2.526 eV. This indicates that the acceptor and donor groups considered in the present study are better than the donor and acceptor groups in the reference dye YD2-o-C8 and can provide a sufficient driving force to enhance the efficiency of electron injection from excited state dye to  $\text{TiO}_2$  surface.

Table 1

#### 3.2. Electronic structure

The ground state structures for the six selected Zn-porphyrin dyes (JC1 – 6) were computed at the B3LYP/ LanL2DZ level. The discussion based on geometrical parameters of the ground state structure was neglected. The highest occupied molecular orbital energies ( $E_{\text{HOMO}}$ ) and the lowest unoccupied molecular orbital energies ( $E_{\text{LUMO}}$ ) along with other quantum chemical parameters of all Zn-porphyrin dyes computed at the B3LYP/ LanL2DZ level was listed in Table 2.

The  $E_{\text{LUMO}}$  level of the sensitizer closely relates to the electron injection efficiency of the  $\text{TiO}_2$  surface. A higher  $E_{\text{LUMO}}$  level is helpful for providing higher electron injection potential and thus, higher electron injection efficiency and higher energy conversion efficiency  $\eta$  [50]. Generally, in dye sensitizers the low  $E_{\text{LUMO}}$  level is matched with the conduction band of  $\text{TiO}_2$ , which limits the further improvement of the energy conversion efficiency of DSSCs. Thus, it is very important to screen novel sensitizer candidates with a higher  $E_{\text{LUMO}}$  level. The  $E_{\text{LUMO}}$  levels of JC1 – 6 sensitizers are between the narrow ranges of

-2.736 to -3.033 eV. These values are more negative than the lower bound level of the conduction band of TiO<sub>2</sub> (-4.0 eV), indicating that there is sufficient thermodynamic driving force for charge injection from the excited sensitizer molecule to the TiO<sub>2</sub> conduction band. Besides the E<sub>LUMO</sub> level, the E<sub>HOMO</sub> level of the sensitizer is also very important for a DSSC, especially for the dye regeneration process [50]. The E<sub>HOMO</sub> energy levels of new zinc-porphyrin sensitizers are in the range of -4.982 to -5.238 eV. This indicates that the  $\pi$  – spacer has a slight influence on E<sub>HOMO</sub> energy level of the dyes. These values are lower than the electrolyte oxidation potential ( $\Gamma/I_3$ : -4.8 eV), ensuring that the driving forces are large enough to efficiently regenerate dyes through the recapture of the injected electrons  $\Gamma$  to the oxidized sensitizers. Although we have compared the E<sub>HOMO</sub> value with the experimental oxidation potential, the theoretical redox potential of the electrolyte is difficult to obtain accurately, so another reference compound is used as a benchmark in assessing the sensitizer candidates. The previously reported dye YD2-o-C8, (see Figure 1) the most effective dye from the Zn-porphyrin sensitizer family, is a good choice as the reference [16]. It is anticipated that sensitizer candidates with an E<sub>HOMO</sub> level close to that of YD2-o-C8 would be promising for dye regeneration since YD2-o-C8 can be regenerated efficiently. From Table 2, we can observe that the E<sub>HOMO</sub> values of dyes JC1 – 3 and JC4 – 6 are higher and lower than reference dye YD2-o-C8, respectively. As a result, the regeneration driving force of JC1 – 3 and JC4 – 6 are lower and higher, respectively, than YD2-o-C8. Generally, it is possible to obtain a higher voltage and higher power conversion efficiencies if the regeneration driving force of the sensitizers is decreased [51]. In the present study we have observed that as the electron donating strength of donor increases the regeneration driving force of the dyes decreases. Therefore, there exists potential to obtain a higher voltage and higher power conversion efficiencies for dyes JC1 – 3 when compared to reference dye YD2-o-C8.

**Table 2**

### 3.3. *Quantum chemical parameters*

The dipole moment and polarizability values calculated at the B3LYP/LanL2DZ level are also presented in Table 2. Dyes with different dipole moments and polarizability can modify the electronic properties of the semiconductors and affect the nature of interaction between dye and acceptor species. The calculated results show that the dipole moments of all the dyes are greater than the reference dye YD2-o-C8. In general, organic dyes with high polarizabilities show strong interaction with surrounding species and induce an increase in the local concentrations of acceptor species [52]. From the Table 2 we can observe that polarizability of dyes JC1 – 3 and JC4 – 6 are greater and smaller than the reference dye YD2-o-C8. Therefore JC1 – 3 at the TiO<sub>2</sub> surface induce an increase in the local concentrations of acceptor species due to their high polarizability (Table 2). The enhancing concentration of acceptor species on the TiO<sub>2</sub> surface increases the possibility of acceptor species penetrating the adsorbed dye layer and leading to electron recombination within a short electron lifetime. The tendency of an electron to escape from a system in its ground state is characterized by the chemical potential ( $\mu$ ). From Table 2, we can also observe that dye JC1 – 3 have the highest chemical potential when compared to YD2-o-C8 and JC4 – 6. This clearly indicates that the electrons in the dyes JC1 – 3 are less likely to escape from a system in equilibrium when compared to JC4 – 6. The chemical hardness ( $\eta$ ) is useful to

investigate generalized Lewis acid/base reactions. A highly polarizable system is expected to be more reactive or softer than a less polarizable system that is expected to be hard and stable. The dyes JC4 – 6 have  $\eta$  values greater than YD2-o-C8, which can be interpreted as the resistance to the charge transfer of the system, JC1 – 3 have  $\eta$  lower than YD2-o-C8, suggesting that their electron density was more readily influenced and that JC1 – 3 would be more reactive than YD2-o-C8. Among all the dyes, JC3 dye has the highest polarizability, indicating a higher field response, due to the higher electron-accepting capacity of its acceptor groups. On the other hand, the capability to accept one electron from a donor is measured by electron affinity, so  $\omega$  may be considered as a kind of “electrophilicity power”. The calculated results show that JC1 – 3 are most electrophilic complexes than YD2-o-C8 and JC4 – 5 dyes have the lowest capability to accept an electron from a donor, showing the lowest values of  $\omega$ .

### 3.4. Energy Gap

In DSSCs, the energy gap is one of the most important properties which affect the photocurrent density of the dye molecule. Mostly, smaller energy gaps render the electrons being more easily excited and thus beneficial for absorbing longer-wavelength light. Hence, more photons can be absorbed at any given time, which may contribute to obtaining a higher short circuit current density  $J_{SC}$  and overall power conversion efficiency  $\eta$  [53]. However, the energy gap of the dye decreases gradually along with the variation of ancillary ligands whose electron-donating abilities are increased, which shows that the powerful electron-donating substituents are very helpful in moving the absorption bands to the longer wavelength side. The energy gap ( $E_g$ ),  $E_{HOMO}$  and  $E_{LUMO}$  energy values of all the dyes are presented in Table 2. The  $E_g$  of the dyes in THF are in increasing order: JC4 > JC5 > JC6 > YD2-o-C8 > JC1 > JC25 > JC3. From our calculations it was found that  $E_{HOMO}$  and  $E_{LUMO}$  energy values of the dyes were obviously affected by the ancillary ligands. The  $E_{HOMO}$  value of JC4 is the lowest among all the investigated compounds in this paper. However, the replacement of bis(4-(hexyloxy)phenyl)amino in JC4 with a 10*H*-phenothiazin-3-yl group leads to the formation of JC1; the latter has the highest  $E_{HOMO}$  value. The  $E_{LUMO}$  value of JC1 – 3 are more negative than the dye YD2-o-C8, whereas the  $E_{HOMO}$  value of these dyes is less negative than the YD2-o-C8. Therefore the sensitizers JC1 – 3 have a smaller  $E_{HOMO}$ – $E_{LUMO}$  gap than that of YD2-o-C8, showing potential for providing red-shifted electronic absorption spectra.

**Figure 2**

**Table 3**

### 3.5. Optical properties

The optical spectra of JC1 – 6 along with the YD2-o-C8 were calculated in THF solvent at the TD – DFT method using C-PCM solvent model. The calculated absorption spectrum of the reference dye YD2-o-C8 using CAM-B3LYP/LanL2DZ along with its experimental results is shown in Figure 2. The experimental absorption spectrum of YD2-o-C8 exhibits three major absorption bands, in which one intense B (Soret) band is observed around 450 nm and two weak Q bands of Q(0,1) and Q(0,0) observed around 580 and 650 nm. Generally, the

long-range-corrected CAM-B3LYP provide the most stable and more reasonable descriptions on the relative intensities and energy level spacing of energy bands, the discrepancy between the calculated and experimental excitation energies were found to be 0.2 eV. Here the vibronic structures are not taken into account. Therefore, the Q(0,1) band is not yielded in the theoretical spectra. The computed vertical excited singlet states and oscillator strengths of dyes JC1 – 6 in THF are presented in the Supporting Information (Tables S1). The absorption in the visible and near-UV region is the most important region for photo-to-current conversion, so only the singlet-singlet transitions of the absorption bands with the wavelength longer than 300 nm were listed in Table S1. The simulated absorption spectra of the six dyes (see Figure 3) and YD2-o-C8 exhibited maxima attributed to the  $\pi \rightarrow \pi^*$  transitions in the range 400 – 550 nm for the Soret band and 550 – 750 nm for the Q band. As expected, the electronic absorption bands of porphyrins are sensitive to push units on the *meso* – position of the porphyrin ring. Replacement of *meso* – substituted diphenylamine unit in YD2-o-C8 by 10*H*-phenothiazin-3-yl unit causes slight changes on the absorption features of the porphyrin dyes. The Soret band of JC1 is slightly red-shifted whereas their Q bands are blue-shifted as compared with the YD2-o-C8. This is attributed to the electronic properties of the two electron donating dioctyloxy substituents at the *ortho*-positions of the *meso* – phenyl ring. However, replacing the 10*H*-phenothiazin-3-yl in JC1 with the bis(4-(hexyloxy)phenyl)amino group leads to the structure JC4, resulting in a red shift and broadening of the absorption bands. The absorption properties of JC1 and JC4 changed significantly as the structures of the electron withdrawing units were varied because there is strong electronic coupling between the electron withdrawing unit and the porphyrin ring, efficiently mediated by the C  $\equiv$  C bond. The anthracene-bridged porphyrins JC3 and JC6 shows red shifts and broadening on the Soret and Q bands compared to the corresponding naphthalene-bridged analogues JC2 and JC5 due to  $\pi$  – extension.

From Figure 3 we can observe that JC4 – 6 shows a red shift, while the remaining dyes JC1 – 3 showing a blue shift when compared to the reference dye YD2-o-C8. The simulated UV-visible spectrum of reference dye YD2-o-C8 shows a first Q(0,0) band at 621 nm (experimental 653 nm), whereas new sensitizers JC1 – 6 show a Q(0,0) band at 602, 607, 613, 644, 648 and 651 nm, respectively. Generally, a dye with a low band gap can generate more electrons in the visible and near infrared regions and enhance the efficiency of DSSCs. But the probability of light absorption by a molecule depends on the molecular extinction coefficient ( $\epsilon$ ). Large values of  $\epsilon$  indicate a high probability of absorption at a given wavelength leading to larger conversion efficiencies [54]. Even though absorption bands of JC1 – 2 are blue shifted their energy gap and molecular extinction coefficients are lower and higher than the reference dye YD2-o-C8. As a result light harvesting efficiency of JC1 – 2 dyes is higher than the reference dye.

For each of the six dyes, the first absorption band results from the electron transitions from HOMO to LUMO. While the intense absorption band near ca. 420 nm in JC1 – 3 is composed of the second transition. For this second transition, the starting orbital is the HOMO-2 or HOMO-3 and the final state is the LUMO or LUMO+1 or LUMO+2 (see Table S1). In order to understand the electronic transitions, the corresponding frontier MOs were examined. The isosurface plots of the MOs, HOMO and LUMO are presented in Figure 4. As observed in Figure 4, the HOMOs of the JC1 – 3 are mainly localized at the electron donating

phenothiazine moiety, whereas for JC4 – 6 the HOMOs are localized on diphenylamine and central porphyrin ring and LUMOs of all the dyes are much more aligned on the porphyrin ring,  $\pi$ -bridge and carboxylic acid, which indicates good electron-separated states. This shows that the HOMOs are located primarily at the donor parts, while the LUMOs are more located at the acceptor moieties. Therefore photoexcited electrons would transfer from the phenothiazine moiety/diphenylamine to the acceptor group during the excitation process, which is of benefit to the injection of the photoexcited electrons to the conduction band of the semiconductor. In support of the assertion of charge transfer character, Figure 4 (bottom) shows charge density difference between the excited and ground states of JC1 – 6 and YD2-o-C8 with yellow regions representing a depletion of density and blue regions denoting an accumulation of density upon excitation. As depicted in Figure 4 (bottom), the density depletion zones (yellow) are mostly located on the conjugation spacer segments, while the regions of density enhancement (blue) are mainly localized on the acceptor moiety which is indicative of an intra-molecular charge transfer when the transition occurs. From Figure 4 we can also observe that the shapes of the HOMOs pertaining to the same donor substituent at the *meso*-position of the zinc-porphyrin core are similar. But the shapes of the LUMOs are different. The difference in shapes of the LUMOs is due to the different strengths of the acceptor groups. Molecular orbital composition of the MOs of the JC1 – 6 along with YD2-o-C8 are given in Table 3. The contribution of  $\pi$ -linker and anchoring groups of our dyes to LUMO is 27-49%, whereas the so far known best dye YD2-o-C8 contributed 25%. Therefore, we may anticipate that the proposed new zinc-porphyrin dyes have more electron coupling with the TiO<sub>2</sub> surface and would be more favorable for electron injection into the TiO<sub>2</sub> surface than the YD2-O-C8 dye.

### 3.6. Factors influencing short-circuit current density ( $J_{SC}$ )

In DSSCs,  $J_{SC}$  can be expressed as [55]

$$J_{SC}(\lambda) = q \int \eta_{IPCE} \phi_{ph}^{source}(\lambda) d\lambda \quad (3)$$

where the monochromatic incident photon – to – current efficiency  $\eta_{IPCE} = LHE \phi_{inject} \eta_{collect}$

$$J_{SC}(\lambda) \approx q \int \frac{LHE(\lambda) \times \lambda \times \phi_{ph}^{source}(\lambda)}{1240} d\lambda$$

Where LHE( $\lambda$ ) is the light harvesting efficiency at a given wavelength,  $\phi_{inject}$  is the electron injection efficiency,  $\eta_{collect}$  denotes the charge collection efficiency and  $\phi_{ph}^{source}(\lambda) = 100 \text{ mW} - \text{cm}^{-2}$  and  $q$  is charge of electron. The light harvesting efficiency (LHE) of the dye has to be as high as possible to maximize the  $J_{SC}$ . Here, LHE is expressed as [55]:

$$LHE = 1 - 10^{-A} = 1 - 10^{-f} \quad (4)$$

where A and f are the absorbance and oscillator strength of the dye associated to the  $\lambda_{max}^{ICT}$ . The oscillator strength is directly derived from the TDDFT calculations and writes [55]

$$f = \frac{2}{3} \lambda_{max}^{ICT} |\vec{\mu}_0 - ICT|^2 \quad (5)$$

where  $\bar{\mu}_0 - ICT$  is the dipolar transition moment associated to the electronic excitation. In order to maximize  $f$ , both  $\lambda_{\max}^{ICT}$  and  $\bar{\mu}_0 - ICT$  must be large. The amount of adsorbed dye on the surface  $\Gamma$  (in mol cm<sup>-2</sup>) can be calculated from the absorbance  $A = 1000 \times \epsilon \times \Gamma$ , where  $\epsilon$  is the molar extinction coefficient (units M<sup>-1</sup> cm<sup>-1</sup>). The Langmuir adsorption isotherm can be written as  $\Gamma = \Gamma_{\max} KC/(1+KC)$ , with  $K$  the binding constant for adsorption,  $\Gamma_{\max}$  the maximum load on TiO<sub>2</sub>, and  $C$  is the dye concentration in the dye bath [56].  $\phi_{inject}$  is related to the driving force  $\Delta G^{inject}$  of electrons injecting from the excited state of dye molecule to the semiconductor substrate. It can be expressed as [55]

$$\Delta G^{inject} = E_{OX}^{dye^*} - E_{CB}^{TiO_2} \quad (6)$$

where  $E_{OX}^{dye^*}$  is the oxidation potential of the dye in the excited state, and  $E_{CB}^{TiO_2}$  is the reduction potential of the semiconductor conduction band. Though it is often difficult to accurately determine  $E_{CB}^{TiO_2}$ , because it is highly sensitive to the conditions, e.g., the pH of the solution, thus we used  $E_{CB}^{TiO_2} = -4.0$  eV [57] which is the experimental value corresponding to conditions where the semiconductor is in contact with aqueous redox electrolytes of fixed pH 7.0 [58, 59]. The excited state oxidation potential ( $E_{OX}^{dye^*}$ ) can be approximated from the redox potential of the ground state ( $E_{OX}^{dye}$ ), [55]

$$E_{OX}^{dye^*} = E_{OX}^{dye} - \lambda_{\max}^{ICT} \quad (7)$$

where  $\lambda_{\max}^{ICT}$  is the energy of the ICT. Note that this relation is only valid if the entropy change during the light absorption process can be neglected.

In addition, based on the Marcus electron transfer theory [60], the total reorganization energy  $\lambda$  could also affect the kinetics of electron injection, which can be approximately described as

$$k_{inject} = A e^{[-\lambda/4k_B T]} \quad (8)$$

where  $A$  is a pre-factor that depends on the strength of electronic coupling between the dye and the surface,  $\lambda$  is the total reorganization energies (the solvent ( $\lambda_s$ ) and internal ( $\lambda_i$ ) reorganization energies),  $k_B$  is the Boltzmann constant and  $T$  is the temperature. Therefore, in order to enhance the  $J_{SC}$  one should focus on improving the LHE and  $\phi_{inject}$  as well as decreasing the reorganization energy ( $\lambda$ ). So we computed the internal reorganization energy  $\lambda_i$  according to the following formula [61]

$$\lambda_i = [E_0^\pm - E_\pm^\pm] + [E_\pm^0 - E_0] \quad (9)$$

where  $E_0^\pm$  is the energy of cation or anion calculated with the optimized structure of the neutral molecule,  $E_\pm^\pm$  is the energy of the cation or anion calculated with the optimized cation or anion structure,  $E_\pm^0$  is the energy of the neutral molecule calculated at the cationic or anionic state, and  $E_0$  is the energy of the neutral molecule at ground state.

**Figure 3**

**Figure 4**

From Figure 3 we can see that all dyes can effectively absorb light in the UV-visible and near-infrared regions with high molar extinction coefficients (more than  $50000 \text{ M}^{-1} \text{ cm}^{-1}$ ). The molecular extinction coefficients of all dyes investigated in this paper are much larger than N3 dye [53] and LHE of the dyes fall within the range: 0.951 – 0.995 (Table 3). For dyes JC1 -3 and JC4 – 6, the calculated oscillator strength decreases as the size of the  $\pi$ -bridge increases from benzene to anthracene, which leads to a decrease in LHE value. The electron injection free energy ( $\Delta G^{\text{inject}}$ ), ground ( $E_{\text{ox}}^{\text{dye}}$ ) and excited ( $E_{\text{ox}}^{\text{dye*}}$ ) state oxidation potentials computed in THF for the six Zn-porphyrin dyes are represented in Table 4. Based on Koopman's theorem [62], the ground state oxidation potential energy is related to ionization potential energy.  $E_{\text{ox}}^{\text{dye}}$  can be estimated as negative of  $E_{\text{HOMO}}$  and  $E_{\text{ox}}^{\text{dye*}}$  is calculated based on Eq. (7) where the columbic stabilization term is neglected. For a favorable electron injection, the calculated energy difference between excited state dye and  $\text{TiO}_2$  conduction band must be more negative. The calculated  $\Delta G^{\text{inject}}$  values of all the dyes JC1 – 6 are more negative ( $< -1.77 \text{ eV}$ ) than the  $\text{TiO}_2$  conduction band edge. From Table 4 we can observe that the  $\Delta G^{\text{inject}}$  values for dyes JC1 – 3 and JC5 – 6 are more negative than the reference dye YD2-o-C8, with the exception of JC4. This indicates that the dye excited states of JC1 – 3 lie more above the  $\text{TiO}_2$  conduction band edge than JC4 and YD2-o-C8 and thus favour more electron injection from dye excited state to the  $\text{TiO}_2$  conduction band edge. The free energy change  $\Delta G^{\text{inject}}$  decreasing in the order JC4 > YD2-o-C8 > JC5 > JC1 > JC2 > JC3 > JC3 from -1.874 to -2.561 eV, indicating that the driving force of the electron injection from the excited states decreases in this order. We found from Table 4 that dyes JC1 – 3 are more exoenergetic free enthalpy of injection ( $< -1.87 \text{ eV}$ ) than YD2-o-C8. Another factor that influences the efficiency of DSSCs is reorganization energy. In order to attain the fast electron transfer the reorganization energy of the sensitizers must be low. Therefore we have calculated reorganization energies for all the dyes and the results are presented in Table 4. The total reorganization energy  $\lambda_i$  for dyes JC1, 2, 4 and 5 are smaller than the reference dye YD2-o-C8. Therefore we can expect to obtain a high electron injection from the excited states to the  $\text{TiO}_2$  conduction band for dyes JC1, 2, 4 and 5 due to their large LHE and low reorganization energy. As a result, the photocurrent response for these dyes is predicted to be higher than that of the reference dye. Therefore, we have calculated  $J_{\text{sc}}$  values using equation 3 by considering approximate parameters  $K \approx 10^4 \text{ M}^{-1}$ ,  $C \approx 10^{-6} \text{ M}$  and  $\Gamma_{\text{max}} \approx 1.5 \times 10^{-7} \text{ mol cm}^{-2}$  for a 6  $\mu\text{m}$  thick  $\text{TiO}_2$  film [56, 63]. The calculated short circuit current density of reference dye YD2-o-C8 compared well with the experimental value of  $17.32 \text{ mA-cm}^{-2}$ . From Table 3, we can observe that  $J_{\text{sc}}$  values for dyes JC1 and JC2 are larger than the reference dye YD2-o-C8, whereas for dyes JC4 and JC5,  $J_{\text{sc}}$  values are slightly lower than the reference dye. This indicates that dye substituted with either 10*H*-phenothiazin-3-yl or bis(4-(hexyloxy)phenyl)amino offer greater potential for DSSC applications.

### 3.7. Dye adsorption on $\text{Ti}_36\text{O}_{72}$

The theoretical study of dye adsorption on the semiconductor surface gives more information regarding electronic structure and optical properties of dyes at the  $\text{TiO}_2$  surface. For binary dye/ $\text{TiO}_2$  calculations, we have considered a  $\text{Ti}_36\text{O}_{72}$  nanocluster, obtained by approximately

cutting an anatase slab to expose the majority (101) surface, as a model of the TiO<sub>2</sub> nanoparticle. In dye – TiO<sub>2</sub> adsorption, the adsorption of dyes through carboxylic acid can be either physisorption or chemisorption. Recently several experimental studies indicate that the carboxylic acid is usually adsorbed on the TiO<sub>2</sub> surface through bidentate bridging [64]. Therefore only bidentate bridging adsorption of JC1 – 6 was presented in this study. Generally, adsorption energy of the dye/TiO<sub>2</sub> system indicates the strength of the interaction between dye and the TiO<sub>2</sub> surface. In DSSCs, the photocurrent density (J<sub>SC</sub>) also depends on the strength of the adsorption energy of dye/TiO<sub>2</sub> system, i.e., the higher the adsorption energy, the stronger the electronic coupling strength between the anchoring group of the dye and the TiO<sub>2</sub> surface, and consequently the larger the J<sub>SC</sub> value is. In order to calculate the adsorption energies of JC1 – 6, they were first fully optimised using the PBE functional together with the double-numerical basis set with polarization performed in the DMol3 program. The optimized structures of YD2-o-C8/(TiO<sub>2</sub>)<sub>36</sub>, JC1/(TiO<sub>2</sub>)<sub>36</sub> and JC4/(TiO<sub>2</sub>)<sub>36</sub> adsorption complexes were shown in Figure 5. Whereas, optimized structures for systems JC2, JC3, JC5 and JC6 are shown in supplementary material (Figure S1). Our calculations show that the sensitizers JC1 – 6 absorb almost perpendicularly to the TiO<sub>2</sub> surface with the formation of two Ti-O bonds. The calculated bond distances between Ti and O atom of dyes are in the range of 1.90 – 2.15 Å. The adsorption energies of JC1 – 6 were predicted to be -13.0, -13.5, -13.9, -14.17, -14.64 and -15.12 kcal/mol, respectively. These values are comparable with the adsorption energy calculated for YD2-o-C8 (E<sub>ads</sub> = -14.1 kcal/mol), indicating a strong interaction between the dyes and the TiO<sub>2</sub> surface. In order to understand the electronic coupling between the LUMO of the dye and the TiO<sub>2</sub> conduction band and the electron transfer features during light excitation, we have performed the single point electronic structure calculations of the optimized structure using B3LYP together with the 3-21G(d) basis set to analyse the frontier MO of the dye – TiO<sub>2</sub> system. Some of the selected isosurfaces for JC1 and reference dye YD2-o-C8 are presented in Figure 6. The HOMO level of the dye/(TiO<sub>2</sub>)<sub>36</sub> system corresponds to the HOMO of the free dye and it is entirely localized on dye, while the LUMO levels of the complex have the same characteristic of the TiO<sub>2</sub> nanoparticle, which is manifest by the charge densities of frontier MOs shown in figure 6. For the (YD2-o-C8)/(TiO<sub>2</sub>)<sub>38</sub> system, the interacting LUMOs have non-negligible contributions from free dye. The free dye LUMO are situated higher up in the conduction band (LUMO+30). However, also for JC1/(TiO<sub>2</sub>)<sub>36</sub> and JC4/(TiO<sub>2</sub>)<sub>36</sub> the interacting orbital shows mixing of dye π\* and TiO<sub>2</sub> 3d orbitals higher up in the conduction band (LUMO+30). This indicates that 10*H*-phenothiazin-3-yl/bis(4-(hexyloxy)phenyl)amino, which acts as the electron donor, inserts its unoccupied MOs deeply into the conduction band of TiO<sub>2</sub> and generates enough driving force for the electron injection from excited dye to TiO<sub>2</sub>.

**Figure 5**

**Figure 6**

**Table 4**

### 3.8. Factors influencing open-circuit voltage (V<sub>OC</sub>)

Besides the J<sub>SC</sub>, the overall power conversion efficiency η is also influenced by the open circuit voltage (V<sub>OC</sub>). In DSSCs, the V<sub>OC</sub> is defined as the potential difference between the

electrolyte redox potential and the quasi-Fermi level of electrons in the semiconductor TiO<sub>2</sub>; the V<sub>OC</sub> can be calculated with the empirical formula given below [65]

$$V_{OC} = \frac{E_C + \Delta CB}{q} + \frac{kT}{q} \ln\left(\frac{n_c}{N_{CB}}\right) - \frac{E_{redox}}{q} \quad (10)$$

Where  $N_{CB}$  is the density of accessible states in the conduction band;  $n_c$  is the number of injected electrons in TiO<sub>2</sub> due to dye adsorption;  $q$  is the charge of electron and  $\Delta CB$  is the shift of  $E_{CB}$  when dyes are adsorbed on TiO<sub>2</sub> and can be expressed as [65]

$$\Delta CB = -\frac{q\mu_{normal}\gamma}{\varepsilon\varepsilon_0} \quad (11)$$

In this expression,  $\mu_{normal}$  denotes the dipole moment of individual dye molecules perpendicular to the surface of the TiO<sub>2</sub>,  $q$  is the charge of electron and  $\gamma$  is the surface concentration of the dye.  $\varepsilon_0$  and  $\varepsilon$  represent the vacuum permittivity and dielectric permittivity, respectively. From equation 10, one can observe that the V<sub>OC</sub> is also influenced by the structure of the dyes. Because the adsorption of the dyes on the semiconductor surface will induce the shift of the TiO<sub>2</sub> conduction band edge. Therefore we have compared the important structural parameters of the dyes before and after the adsorption on TiO<sub>2</sub> surface calculated at the same level of theory (GGA/PBE/DNP). The important structural parameters of dyes are presented in Figure S2 – S8. From Figures S2 – S8, we can observe that there are slight changes in structural parameters of porphyrin core and donor units, but noticeable changes have been observed in the acceptor region of the dye when placed on the TiO<sub>2</sub> surface. It is also obvious from the Equations (10) and (11) that a dye with large  $\mu_{normal}$  exerts a crucial influence on the V<sub>OC</sub>. The calculated results show that the dyes are almost perpendicularly adsorbed onto the TiO<sub>2</sub> surface and total dipole moments are making an angle of roughly 45° with the TiO<sub>2</sub> surface. The total dipole moments calculated at B3LYP/3-21G(d) in THF solvent are 13.94, 19.58, 35.96, 17.37, 31.74 and 24.69 Debyes for JC1 – 6, respectively. Whereas the dipole moment is calculated to be 13.55 Debye for YD2-o-C8. The calculated results shown that all the dye/(TiO<sub>2</sub>)<sub>36</sub> systems have dipole moments larger than the reference system YD2-o-C8, as a result the conduction band edge of the TiO<sub>2</sub> system shifted towards higher energy levels. In order to verify this we have presented the energy level alignment of the dye – TiO<sub>2</sub> systems in Figure 7. The molecular energy levels (see figure 7) show that the conduction band edge of the dye - TiO<sub>2</sub> systems shifted to higher energy levels but the shift is slightly larger than the YD2-o-C8 – TiO<sub>2</sub> system. Therefore, the results indicate that there is a negligible deviation between V<sub>OC</sub> of dyes (JC1 – 6) and reference dye YD2-o-C8. Although it is reported that the calculated  $\Delta CB$  could fit the experimental V<sub>OC</sub>, but the results obtained with the above equation 11 are still in debate, i.e., the calculated conduction band shift directly cannot estimate the V<sub>OC</sub> performance in DSSCs. Therefore, another parameter such as excited state life time of the dye is also more useful to understand the performance of DSSCs [52].

### 3.9. Excited state lifetimes ( $\tau$ )

The singlet excited state lifetime is one of the important properties of dye sensitizers, which can be useful to estimate the efficiency of electron injection to the TiO<sub>2</sub>. Electron injection from the excited dye to the semiconductor occurs within 100 fs. This fast injection means that

increasing concentration of acceptor species on the TiO<sub>2</sub> surface increases the possibility of acceptor species penetrating the adsorbed dye layer, leading to electron recombination, which results in a short electron lifetime. This lowers the photovoltage and reduces the efficiency of charge collection, decreasing the short circuit photocurrent density and photo current efficiency. After the electron injection, the dye is in a cationic state until regeneration by a redox mediator occurs. The timescale of this regeneration is 100 ns – 1 μs. To realize long-term stability, the dyes must remain stable in the cationic form for a long time. Recently, Mozer *et al.*, have reported that a remarkably reduced electron lifetime in porphyrin based DSSCs is the main reason for the generally lower V<sub>OC</sub> than for the Ru sensitizer N719 [66]. In order to calculate the excited state lifetimes, we optimised the geometries of the molecules in the first excited singlet electronic state and investigated the lowest excitation energy and corresponding oscillator strength with the TD-B3LYP/LANL2DZ method. The excited state lifetimes of the dye sensitizers were then calculated using the formula:  $\tau = 1.499 / (f E^2)$ , where E is the excitation energy of the different electronic states (cm<sup>-1</sup>) and f is oscillator strength of the electronic state. The results are presented in Table 4. The calculated results show that the excited state lifetime for JC1 – 6 were significantly larger than that of reference dye YD2-o-C8, respectively. However, an increase in lifetimes of JC1 – 6 will retard the charge recombination process and enhance the efficiency of the DSSCs.

### 3.10. Level alignment quality ( $\eta$ )

Recently, Ørnsø *et al.*, [67] introduced a no-loss DSSC level alignment quality to screen the functionalized zinc porphyrin for DSSCs applications, which is defined as

$$\eta = \frac{V_{OC} \int_{E_c - E_H}^{\infty} \Theta(E - E_1) J_{SC}(E) dE}{\int_0^{\infty} E \cdot \phi_{ph}^{source} dE}$$

where

$$\Theta(E - E_1) = \begin{cases} 1 & \text{for } E - E_1 \geq 0 \\ 0 & \text{for } E - E_1 < 0 \end{cases}$$

Here  $E_c - E_H$  is the distance from the HOMO level to the conduction band,  $E_1$  is the optical gap of the dye,  $\Theta(E - E_1)$  is a step function representing the absorption of the dye molecules,

$J_{SC}(E)$  is the short-circuit current density and  $\int_0^{\infty} E \cdot \phi_{ph}^{source} dE = 100 \text{ mW} / \text{cm}^2$ . Therefore we

have calculated the level alignment quality for the dyes JC1 – JC6 using the above equation by considering two different models for open circuit voltage i.e.,  $V_{oc} = E_c - E_H$  and  $V_{oc} = 1 \text{ V}$  [67]. The calculated results presented in Table 5 show that the  $\eta$  value obtained for dyes substituted with 10*H*-phenothiazin-3-yl and acene bridged (benzene and naphthalene) carboxylic acid (JC1 – 2) are larger than the reference dye. Whereas for dyes JC4 – 6,  $\eta$  value is lower than the reference dye YD2-o-C8. These results clearly indicate that as the conjugation of the  $\pi$ -spacer increases the  $\eta$  value of the dyes are decreasing due to dye aggregation. Based on above results, we conclude that Zn-porphyrin dyes substituted with 10*H*-phenothiazin-3-yl donor group offer more potential for DSSCs application.

### 3.11. Nonlinear optical properties

Nonlinear optical (NLO) properties play a vital role in the design of new dyes, since they not only mirror the degree of noncentrosymmetry, but also characterize the ability of the compound to undergo  $\pi$ -electron delocalization and intramolecular charge transfer, which are required for efficient electron injection from the dye to the semiconductor in DSSCs [68]. The intra-molecular charge transfer band associated with molecules which exhibit an extended polarized  $\pi$  electron system is most often an isolated  $\pi \rightarrow \pi^*$  transition. This absorption band is characterized by a large change in the dipole moments of the ground and excited state. According to Oudar *et al.*, [69] the charge transfer contribution to the second-order nonlinearity in the two-level approximation can be written as

$$\beta_{CT} = \frac{3e^2 h^2 W f \Delta\mu}{8\varepsilon_0 \pi^2 m [W^2 - (2h\nu)^2] \cdot [W^2 - (h\nu)^2]} \quad (12)$$

with  $\Delta\mu = \mu_e - \mu_g$  being the difference between the excited and ground state dipole moment,  $h\nu$  the photon energy of the laser,  $f$  the oscillator strength of the charge transfer transition,  $e$  and  $m$  the electron charge and mass, and  $W$  the energy of the maximum of the charge transfer absorption band. In the present study, the tensor components of the nonlinear response  $\beta$  were analytically calculated in THF solution by using the coupled perturbed Hartree-Fock (CPHF) method which is implemented in Gaussian 03 program. The intrinsic hyperpolarizability  $\beta_{tot}$  is given by the magnitude of the vector component of the hyperpolarizability ( $\beta$ );  $\beta_{tot} = \sqrt{\beta_x^2 + \beta_y^2 + \beta_z^2}$ , where  $x$ ,  $y$  and  $z$  are the vector components of the hyperpolarizability tensor in the direction of the  $x$ ,  $y$  and  $z$  molecular axis, respectively [70]. The calculated values were converted into electrostatic units (1 a.u. =  $8.6398 \times 10^{-33}$  esu). The values of the first hyperpolarizabilities ( $\beta$ ) were summarized in Table 4.

The magnitude of the tensor component of the first-order hyperpolarizability can be used to assess the charge transfer character of certain analogues. Because only one tensor component dominates the NLO response of the system, this suggested that these dyes would undergo a unidirectional charge transfer transition from the donor to acceptor groups, which is ideal in DSSC applications. All of the dyes studied in this paper have a charge transfer axis along the  $X$  – direction (see Figure 1). The calculated  $\beta_{xxx}$  values in Table 4 are consistent with the donor and acceptor strengths of the dyes. The calculated results show that  $\beta_{xxx}$  values of JC4 – 6 are lower than and the values of JC1 – 3 are higher than the value for the reference dye YD2-o-C8. The calculated results show that that  $\beta_{xxx}$  was greatly influenced by the character of the donor and acceptor groups. This demonstrates the dyes substituted with 10*H*-phenothiazin-3-yl are potential for DSSC applications.

#### 4.0. CONCLUSIONS

The electronic and optical properties of six Zn porphyrin dyes (JC1 – 6) substituted with either 10*H*-phenothiazin-3-yl or bis(4-(hexyloxy)phenyl)amino and acene bridged carboxylic acid as an electron donating and accepting units were studied using DFT and TDDFT methods. Excitation energies were calculated in THF for each dye, using TDDFT with the CAM-B3LYP/LanL2DZ method. The adsorption energies of dyes adsorbed on the  $(\text{TiO}_2)_{36}$  cluster was calculated with DFT calculations using DMol<sup>3</sup> program and found that JC1 – 6 dyes are more stable and have an adsorption energy similar to complex YD2-o-C8. The

acceptor and donor groups considered in the present study are better than that of the reference dye YD2-o-C8 and provide a sufficient driving force to enhance the efficiency of electron injection from excited state dye to TiO<sub>2</sub> surface. The Zn-porphyrin sensitizers with the diphenylamine substituents at *meso*-positions (i.e., dyes JC4 – 6) have a higher E<sub>HOMO</sub> energy level and results a smaller regeneration driving force than YD2-o-C8. The calculated dipole moments for all the dyes are larger than that of YD2-o-C8, especially for dyes containing the naphthalene moiety as the  $\pi$ -linker. The calculated energy gaps of the dyes in THF are in decreasing order: JC1 > JC2 > JC3 > YD2-o-C8 > JC4 > JC5 > JC6. Therefore the predicted sensitizers JC4 – 6 have a smaller energy gap than that of YD2-o-C8, showing the potential of providing red-shifted electronic absorption spectra. The simulated absorption spectra of the six dyes and YD2-o-C8 exhibited maxima attributed to the  $\pi \rightarrow \pi^*$  transitions in the range 400 – 550 nm for the Soret band and 550 – 750 nm for the Q band. We have observe that replacement of the *meso*-substituted diphenylamine unit in YD2-o-C8 by either 10*H*-phenothiazin-3-yl or a bis(4-(hexyloxy)phenyl)amino unit causes a blue or red shift, respectively. The calculated results show that Zn-porphyrin dyes substituted with 10*H*-phenothiazin-3-yl donor and either 4-ethynylbenzoic acid or 4-ethynyl-1-naphthoic acid offer potential for use in DSSCs due to their larger molecular excitation coefficient, excited state lifetime, LHE, J<sub>SC</sub>, level alignment quality and smaller electron reorganization energy than the reference dye.

## SUPPORTING INFORMATION

Contains singlet excitation energies, oscillator strengths, reorganization energy and first hyperpolarizability values of all the dyes calculated at the B3LYP/Lan12dz level of theory.

## ACKNOWLEDGMENTS

The authors thank the National Science Foundation of China for supporting this work under Grant no. 21372116.

## REFERENCES

1. J. Oh, H. C. Yuan, H. M. Branz, *Nature Nanotechnology*, 2012, 7, 743–748.
2. R. Knodler, J. Sopka, F. Harbach, H. W. Grunling, *Sol. Energy Mater. Sol. Cells*, 1993, 30, 277–281.
3. A. Kay, M. Gratzel, *Sol. Energy Mater. Sol. Cells*, 1996, 44, 99–117.
4. H. Pettersson, T. Gruszecki, *Sol. Energy Mater. Sol. Cells*, 2001, 70, 203–212.
5. S. Y. Dai, K. J. Wang, J. Weng, Y.F. Sui, Y. Huang, S. F. Xiao, S.H. Chen, L. H. Hu, F.T. Kong, X. Pan, C. W. Shi, L. Guo, *Sol. Energy Mater. Sol. Cells*, 2005, 85, 447–455.
6. B. A. Gregg, *J. Phys. Chem.*, 1996, 100, 852–859.
7. K. Hara, T. Sato, R. Katoh, A. Furube, Y. Ohga, A. Shinpo, S. Suga, K. Sayama, H. Sugihara, H Arakawa, *J. Phys. Chem. B*, 2003, 107, 597–606.
8. K. Sayama, S Tsukagoshi, K. Hara, Y. Ohga, A. Shinpou, Y. Abe, *J. Phys. Chem. B.*, 2002, 106, 1363–1371.
9. K. Hara, M. Kurashige, Y. Dan, C. Kasada, A. Shinpo, S. Saga, *New. J. Chem.*, 2003, 27, 783–785.
10. H. Tokuhisa, P.T. Hammond, *Adv. Fun. Mater.*, 2003, 13, 831–839.
11. T. Horiuchi, H. Miura, S. Uchida, *J. Am. Chem. Soc.*, 2004, 126, 12218–12219.

12. A. Mishra, M. K. R. Fischer, P. Bauerle, *Angew. Chem. Int. Ed.*, 2009, 48, 2474–2499.
13. A. Hagfeldt, G. Boschloo, L. Sun, L. Kloo, H. Pettersson, *Chem. Rev.*, 2010, 110, 659–6663.
14. Y. Ooyama, Y. Harima, *Eur. J. Org. Chem.*, 2009, 2903–2934.
15. M. G. Walter, A. B. Rudine, C. C. Wamser, *J. Porphyrins Phthalocyanines*, 2010, 14, 759–792.
16. A. Yella, H. W. Lee, H. N. Tsao, C. Yi, A. K. Chandiran, M. K. Nazeeruddin, E. W. G. Diao, C. Y. Yeh, S. M. Zakeeruddin, M. Grätzel, *Science*, 2011, 334, 629–634.
17. B. E. Hardin, H. J. Snaith, M. D. McGehee, *Nature Photonics*, 2012, 6, 162–169.
18. P. J. Spellane, M. Gouterman, A. Antipas, S. Kim, Y. C. Liu, *Inorg. Chem.* 1980, 19, 386–391.
19. E. M. Barea, R. Caballero, L. L. A. A. Guerrero, P. L. Cruz, F. Langa, J. Bisquert, *Chem Phys Chem.*, 2011, 12, 961–965.
20. L. Giribabu, K. Ravi Kumar, *Current Science*, 2013, 104, 847–855.
21. T. Bessho, S. M. Zakeeruddin, C. Y. Yeh, E. W. G. Diao, M. Gratzel, *Angew. Chem. Int. Ed.*, 2010, 49, 6646–6649
22. B. Liu, W. Zhu, Y. Wang, W. Wu, X. Li, B. Chen, Y. T. Long, Y. Xie, *J. Mater. Chem.*, 2012, 22, 7434–7444.
23. J. Liu, X. Yang, L. Sun, *Chem. Commun.*, 2013, 49, 11785–11787.
24. W. M. Campbell, K. W. Jolley, P. Wagner, K. Wagner, P. J. Walsh, K. C. Gordon, L. S. Mende, M. K. Nazeeruddin, Q. Wang, M. Gratzel, D. L. Officer, *J. Phys. Chem. C*, 2007, 111, 11760–11762
25. Eva M. Barea, V. G. Pedro, T. R. Sanchis, H. P. Wu, L. L. Li, C. Y. Yeh, E. W. G. Diao, J. Bisquert, *J. Phys. Chem. C*, 2011, 115, 10898–10902
26. T. R. Sanchis, B. C. Guo, H. P. Wu, T. Y. Pan, H. W. Lee, S. R. Raga, F. F. Santiago, J. Bisquert, C. Y. Yeh, E. W. G. Diao, *Chem. Commun.*, 2012, 48, 4368–4370.
27. S. M. LeCours, S. G. DiMagno, M. J. Therien, *J. Am. Chem. Soc.*, 1996, 118, 11854–11864.
28. L. L. Li, E. W. G. Diao, *Chem. Soc. Rev.*, 2013, 42, 291–304
29. M. V. M. Diaz, G. D. L. Torrea, Tomas Torres, *Chem. Commun.*, 2010, 46, 7090–7108.
30. H. Imahori, T. Umeyama, S. Ito, *Acc. Chem. Res.*, 2009, 42, 1809–1818.
31. R. Ma, P. Guo, H. Cui, X. Zhang, M. K. Nazeeruddin, M. Gratzel, *J. Phys. Chem. A*, 2009, 113, 10119–10124.
32. M. Pastore, E. Mosconi, F. D. Angelis, M. Gratzel, *J. Phys. Chem. C*, 2010, 114, 7205–7212.
33. M. G. Ju, W. Z. Liang, *J. Phys. Chem. C* 2013, 117, 14899–14911.
34. R. Ma, P. Guo, H. Cui, X. Zhang, M. K. Nazeeruddin, M. Gratzel, *J. Phys. Chem. A*, 2009, 113, 10119–10124.
35. F. Yang, Z. Zhanga, X. He, *Dalton Trans.*, 2013, 42, 13874–13881.
36. L. Ye, *Chin. Sci. Bull.*, 2008, 53, 3615–3619.
37. S. Jungstittiwong, R. Tarsang, T. Sudyoadsuk, V. Promarak, P. Khongpracha, S. Namuangruk, *Org. Electronics*, 2013, 14, 711–722.
38. S. Zalis, R. F. Winter, W. Kaim, *Coord. Chem. Rev.*, 2010, 254, 1383–1396.
39. N. M. Reddy, T. Y. Pan, Y. C. Rajan, B. C. Guo, C. M. Lan, E. W. G. Diao, C. Y. Yeh, *Phys. Chem. Chem. Phys.*, 2013, 15, 8409–8415.
40. C. L. Wang, C. M. Lan, S. H. Hong, Y. F. Wang, T. Y. Pan, C. W. Chang, H. H. Kuo, M. Kuo, E. W. G. Diao, C. Y. Lin, *Energy Environ. Sci.*, 2012, 5, 6933–6940
41. S. Mathew, A. Yella, P. Gao, R. H. Baker, B. F. E. Curchod, N. A. Astani, I. Tavernelli, U. Rothlisberger, M. K. Nazeeruddin, M. Grätzel, *Nat. Chem*, 2014, 1755–4349
42. M. J. Frisch, G. W. Trucks, H. B. Schlegel, G. E. Scuseria, M. A. Robb, J. R. Cheeseman, J. A. Montgomery Jr., T. Vreven, K. N. Kudin, J. C. Burant, J. M. Millam, S. S. Iyengar, J.

- Tomasi, V. Barone, B. Mennucci, M. Cossi, G. Scalmani, N. Rega, G. A. Petersson, H. Nakatsuji, M. Hada, M. Ehara, K. Toyota, R. Fukuda, J. Hasegawa, M. Ishida, T. Nakajima, Y. Honda, O. Kitao, H. Nakai, M. Klene, X. Li, J. E. Knox, H. P. Hratchian, J. B. Cross, V. Bakken, C. Adamo, J. Jaramillo, R. Gomperts, R. E. Stratmann, O. Yazyev, A. J. Austin, R. Cammi, C. Pomelli, J. W. Ochterski, P. Y. Ayala, K. Morokuma, G. A. Voth, P. Salvador, J. J. Dannenberg, V. G. Zakrzewski, S. Dapprich, A. D. Daniels, M. C. Strain, O. Farkas, D. K. Malick, A. D. Rabuck, K. Raghavachari, J. B. Foresman, J. V. Ortiz, Q. Cui, A. G. Baboul, S. Clifford, J. Cioslowski, B. B. Stefanov, G. Liu, A. Liashenko, P. Piskorz, I. Komaromi, R. L. Martin, D. J. Fox, T. Keith, M. A. Al-Laham, C. Y. Peng, A. Nanayakkara, M. Challacombe, P. M. W. Gill, B. Johnson, W. Chen, M. W. Wong, C. Gonzalez, and J. A. Pople, Gaussian 03, Revision E.01, Gaussian, Inc., Wallingford CT, 2004.
43. P. J. Hay, W. R. Wadt, *J. Chem. Phys.*, 1985, *82*, 299–310
  44. J. Koseki, R. Maezono, M. Tachikawa, M. D. Towler, R. J. Needs, *J. Chem. Phys.*, 2008, *129*, 085103–085107.
  45. T. Yanai, D. P. Tew, N. C. Handy, *Chem. Phys. Lett.*, 2004, *393*, 51–57
  46. M. Szafran, M. M. Karelson, A. R. Katritzky, J. Koput, M. C. Zerner, *J. Comput. Chem.*, 1993, *14*, 371–377
  47. Y. Wang, H. Li, *J. Chem. Phys.*, 2010, *133*, 034108/1-11
  48. B. Delley, *J. Chem. Phys.*, 2000, *113*, 7756–7764.
  49. W. Zeng, T. Liu, Z. Wang, S. Tsukimoto, M. Saito, Y. Ikuhara, *Materials Transactions*, 2010, *51*, 171–175
  50. E. M. Barea, C. Zafer, B. Gultekin, B. Aydin, S. Koyuncu, S. Leli, F. F. Santiago, J. Bisquert, *J. Phys. Chem. C*, 2010, *114*, 19840–19848.
  51. S. M. Feldt, P. W. Lohse, F. Kessler, M. K. Nazeeruddin, M. Gratzel, G. Boschloo, A. Hagfeldt, *Phys. Chem. Chem. Phys.*, 2013, *15*, 7087–7097
  52. J. I. Nishida, T. Masuko, Y. Cui, K. Hara, H. Shibuya, M. Ihara, T. Hosoyama, R. Goto, S. Mori, Y. Yamashita, *J. Phys. Chem. C*, 2010, *114*, 17920–17925
  53. M. K. Nazeeruddin, A. Kay, Rodicio, R. Humpbry-Baker, E. Miiller, P. Liska, N. Vlachopoulos, M. Gratzel, *J. Am. Chem. Soc.*, 1993, *115*, 6382–6390.
  54. M. G. Neumann, W. G. M. C. C. Schmitt, F. A. Rueggeberg, I. C. Correa, *Journal of Dentistry*, 2005, *33*, 525–532
  55. J. Feng, Y. Jiao, W. Ma, M. K. Nazeeruddin, M. Gratzel, S. Meng, *J. Phys. Chem. C* 2013, *117*, 3772–3778
  56. M. Pazoki, P. W. Lohse, N. Taghavinia, A. Hagfeldt, G. Boschloo, *Phys. Chem. Chem. Phys.*, 2014, *16*, 8503–8508
  57. J. B. Asbury, Y. Q. Wang, E. Hao, H. Ghosh, T. Lian, *Res. Chem. Intermed.*, 2001, *27*, 393–406.
  58. R. Katoh, A. Furube, T. Yoshihara, K. Hara, G. Fujihashi, S. Takano, S. Murata, H. Arakawa, M. Tachiya, *J. Phys. Chem. B*, 2004, *108*, 4818–4822.
  59. A. Hagfeldt, M. Gratzel, *Chem. Rev.*, 1995, *95*, 49–68.
  60. R. A. Marcus, *Rev. Mod. Phys.*, 1993, *65*, 599–530.
  61. V. Vaissier, P. Barnes, J. Kirkpatrick, J. Nelson, *Phys. Chem. Chem. Phys.*, 2013, *15*, 4804–4814
  62. T. A. Koopmans, *Physica*, 1933, *1*, 104–113.
  63. A. S. Hart, C. B. KC, H. B. Gobeze, L. R. Sequeira, F. D'Souza, *ACS Appl. Mater. Interfaces* 2013, *5*, 5314–5323

64. M. K. Nazeeruddin, R. H. Baker, P. Liska, M. Grätzel, *J. Phys. Chem. B*, 2003, *107*, 8981–8987
65. W. L. Ding, D. M. Wang, Z. Y. Geng, X. L. Zhao, Y. F. Yan, *J. Phys. Chem. C* 2013, *117*, 17382–17398
66. A. J. Mozer, P. Wagner, D. L. Officer, G. G. Wallace, W. M. Campbell, M. Miyashita, K. Sunahara, S. Mori, *Chem. Commun.*, 2008, 4741–4743
67. K. B. Ørnsø, J. M. G. Lastraa, K. S. Thygesena, *Phys. Chem. Chem. Phys.*, 2013, *15*, 19478—19486
68. J. M. Cole, *Complex Systems*, 2011, *20* 141 – 149
69. J. L. Oudar, D. S. Chemla, *J. Chem. Phys.*, 1977, *66*, 2664-2668
70. K. S. Thanthiriwatte, K.M. N. de Silva, *J. Mol. Struct. (Theochem)*., 2002, *617*, 169–175

### List of Figures

**Figure 1.** Chemical structures of reference dye YD2-o-C8 and modeled Zn-porphyrin dyes

**Figure 2.** Comparison of experimental and calculated absorption spectrum of YD2-o-C8 dye in THF solution.

**Figure 3.** Calculated absorption spectra for the JC1 – 6 dyes in THF solution at the C-PCM – TDCAM – B3LYP/ LanL2DZ level of theory.

**Figure 4.** HOMO, LUMO, and electron density difference maps (EDDM) between the excited and ground states of JC1 – 6 and YD2-o-C8 dyes. The contour thresholds for molecular orbitals and density differences are 0.01 and 0.0001 a.u., respectively. The yellow and blue colors indicate a decrease and increase of charge densities, respectively.

**Figure 5.** Optimized bidentate chelate bridging mode of YD2-o-C8, JC1 and JC4 dyes on the  $(\text{TiO}_2)_{36}$  cluster calculated by PBE/DNP on DMol3 program.

**Figure 6.** (a) HOMO (b) LUMO and (c) interacting orbital isosurfaces of reference dye YD2-o-C8 and JC1 dyes on the  $(\text{TiO}_2)_{36}$  nanoparticle. The isovalue is 0.001 a.u.

**Figure 7.** Energy level diagram of dye –  $\text{TiO}_2$  systems investigated in the present study.

### List of Tables

**Table 1.** HOMOs and LUMOs of Donor (D) and acceptor (A) in Different Dyes calculated using B3LYP/6-311G(d,p) method.

**Table 2.** Calculated  $E_{\text{HOMO}}$ ,  $E_{\text{LUMO}}$  levels, Energy gap ( $E_g$ ), dipole moment ( $\rho$ ), Polarizability ( $\alpha$ ) and other quantum chemical parameters electronegativity ( $\chi$ ), chemical potential ( $\mu$ ), chemical hardness ( $\eta$ ) and electrophilicity power  $\omega$  values of Zn-porphyrin based sensitizers at the B3LYP/LanL2DZ level

**Table 3.**

Percentage (%) molecular orbital contribution of the HOMO and LUMO, light harvesting efficiency (LHE) and short circuit current density ( $J_{\text{SC}}$ ) of the Zn-porphyrin based sensitizers in THF solvent at the CAM-B3LYP/LanL2DZ level.

**Table 4.** Excitation energy (E), oscillator strength (f), redox potentials ( $E_{\text{dye ox}}$  and  $E_{\text{dye}^* \text{ox}}$ ),  $\Delta G_{\text{inject}}$ , total internal reorganization energy ( $\lambda_{\text{total}}$ ), excited state lifetime ( $\tau$ ) and first hyperpolarizability ( $\beta$ ) for the JC1 – 6 dyes calculated using B3LYP/LanL2DZ level.

**Table 5.** Calculated  $E_c - E_H$ ,  $E_1$  and  $\eta$  values for six Zn-porphyrin dyes

**Table 1.** HOMOs and LUMOs of isolated Donor (D) and acceptor (A) units in Different Dyes calculated using B3LYP/6-311G(d,p) method.

	$E_{\text{HOMO}}$ (eV)	$E_{\text{LUMO}}$ (eV)
D1	-4.825	-0.406
D2	-4.519	-0.436
D3	-4.770	-0.691
A1	-7.401	-1.868
A2	-6.273	-2.148
A3	-5.617	-2.526

**Table 2.** Calculated  $E_{\text{HOMO}}$ ,  $E_{\text{LUMO}}$  levels, Energy gap ( $E_g$ ), dipole moment ( $\rho$ ), Polarizability ( $\alpha$ ) and other quantum chemical parameters electronegativity ( $\chi$ ), chemical potential ( $\mu$ ), chemical hardness ( $\eta$ ) and electrophilicity power  $\omega$  values of Zn-porphyrin based sensitizers at the B3LYP/Lan12DZ level

Molecule	$E_{\text{LUMO}}$ (eV)	$E_{\text{HOMO}}$ (eV)	$E_g$ (eV)	$\chi$ (eV)	$\mu = -\chi$ (eV)	$\eta$ (eV)	$\omega = \mu^2/2\eta$ (eV)	$\rho$ (Debye)	$\alpha$ (a.u)
YD2-o-C8	-2.955	-5.083	2.128	4.019	-4.019	2.128	3.795	2.192	1391
JC-1	-2.951	-4.964	2.013	3.957	-3.957	2.013	3.889	3.815	1416
JC-2	-3.013	-4.969	1.955	3.991	-3.991	1.955	4.073	4.770	1481
JC-3	-3.047	-4.959	1.911	4.003	-4.003	1.911	4.192	4.501	1538
JC-4	-2.927	-5.238	2.310	4.082	-4.082	2.310	3.605	3.304	1310
JC-5	-2.987	-5.230	2.242	4.108	-4.108	2.242	3.762	4.358	1374
JC-6	-3.033	-5.215	2.182	4.124	-4.124	2.182	3.897	3.063	1425

**Table 3.** Percentage (%) molecular orbital contribution of the HOMO and LUMO, light harvesting efficiency (LHE) and short circuit current density ( $J_{SC}$ ) of the Zn-porphyrin based sensitizers in THF solvent at the CAM-B3LYP/LanL2DZ level.

Dye		E (eV)	$E_g$ (eV)	Acceptor (%)		Donor (%)		$\lambda_{max}$ (nm) / $\epsilon$ (cm <sup>-1</sup> M <sup>-1</sup> )	LHE*	$J_{SC}$ * (mA-cm <sup>-2</sup> )
				Porphyrin linker	$\pi$ - linker + Anchoring group	phenothiazin-3-yl / diphenylamine	Ancillary ligand			
YD2-o-C8	HOMO	-6.29	4.01	35	6	58	1	419 / 222183	0.986	18.10 (17.3 exp)
	LUMO	-2.28		72	25	2	1	620 / 29301		
JC-1	HOMO	-6.37	4.13	58	11	28	2	427 / 261298	0.995	20.46
	LUMO	-2.25		70	27	2	1	602 / 28186		
JC-2	HOMO	-6.36	4.07	60	14	24	2	438 / 235848	0.995	19.68
	LUMO	-2.29		59	38	2	1	607 / 33735		
JC-3	HOMO	-6.33	4.00	57	22	20	2	469 / 107428	0.959	11.72
	LUMO	-2.33		49	49	1	0	613 / 40658		
JC-4	HOMO	-6.07	3.89	22	3	74	1	410 / 211314	0.991	17.12
	LUMO	-2.18		70	27	3	1	624 / 30549		
JC-5	HOMO	-6.08	3.85	22	4	74	1	423 / 208506	0.990	17.51
	LUMO	-2.23		60	37	2	1	629 / 35831		
JC-6	HOMO	-6.06	3.80	24	5	71	1	456 / 127334	0.951	13.08
	LUMO	-2.26		49	48	2	0	636 / 39994		

\* LHE =  $1 - 10^{-f}$  and  $J_{SC}$  calculated for maximum absorption peak.

**Table 4.** Excitation energy (E), oscillator strength (f), redox potentials ( $E_{\text{dye ox}}$  and  $E_{\text{dye}^* \text{ox}}$ ),  $\Delta G_{\text{inject}}$ , total internal reorganization energy ( $\lambda_{\text{total}}$ ), excited state lifetime ( $\tau$ ) and first hyperpolarizability ( $\beta$ ) for the JC1 – 6 dyes calculated using B3LYP/Lanl2DZ level.

Molecule	E (cm <sup>-1</sup> )	f	$E_{\text{dye ox}}$ (eV)	$E_{\text{dye}^* \text{ox}}$ (eV)	$\Delta G_{\text{inject}}$ (eV)	$\tau$ (ns)	$\lambda_e$ (eV)	$\lambda_h$ (eV)	$\lambda_i$ (eV)	$\beta_{\text{xxx}}$ (a.u)
YD2-o-C8	23092	1.18	5.08	2.12	-1.87	2.38	0.265	0.207	0.472	20036
JC-1	22094	1.28	4.96	1.85	-2.14	2.39	0.224	0.239	0.463	67405
JC-2	22690	0.87	4.96	1.71	-2.28	3.36	0.224	0.243	0.467	77692
JC-3	20174	0.31	4.95	1.43	-2.56	12.0	0.326	0.324	0.650	74674
JC-4	22665	1.15	5.23	2.22	-1.77	2.53	0.236	0.227	0.463	14414
JC-5	21665	1.15	5.23	2.13	-1.86	2.79	0.245	0.218	0.463	15844
JC-6	20030	0.42	5.21	1.90	-2.09	8.91	0.318	0.211	0.529	13506

**Table 5.** Calculated  $E_c - E_H$ ,  $E_1$  and  $\eta$  values for six Zn-porphyrin dyes

Dye	$E_c - E_H$ (eV)	$E_1^a$ (eV)	$\eta_{\text{con}}^b$	$\eta_{\text{dyn}}^c$
YD2-o-C8	2.39	2.96	0.43	0.53
JC 1	2.27	2.90	0.46	0.59
JC 2	2.29	2.83	0.45	0.55
JC 3	1.75	2.64	0.21	0.30
JC 4	2.27	3.02	0.39	0.51
JC 5	2.36	2.93	0.41	0.51
JC 6	2.26	2.72	0.30	0.35

<sup>a</sup> optical band gap calculate by  $E_1 = 1240 \text{ eV} / \lambda$ , where  $\lambda$  absorption maximum of dye calculated at the CAM-B3LYP/Lanl2DZ level.

<sup>b</sup>  $V_{\text{oc}} = 1 \text{ V}$ .

<sup>c</sup>  $V_{\text{oc}} = E_c - E_H$ .

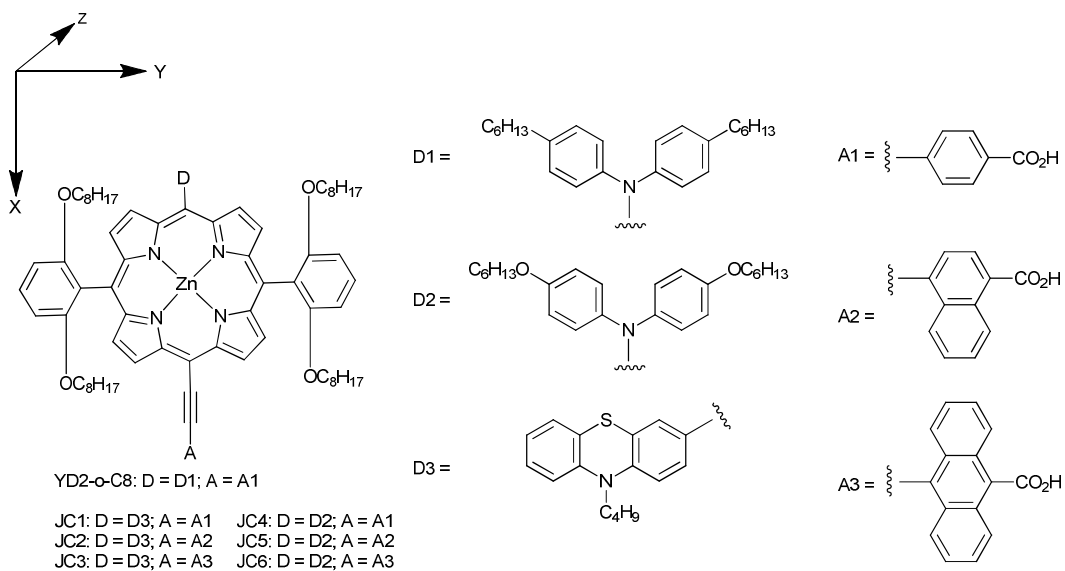


**Figure 1.** Chemical structures of reference dye YD2-o-C8 and modeled Zn-porphyrin dyes

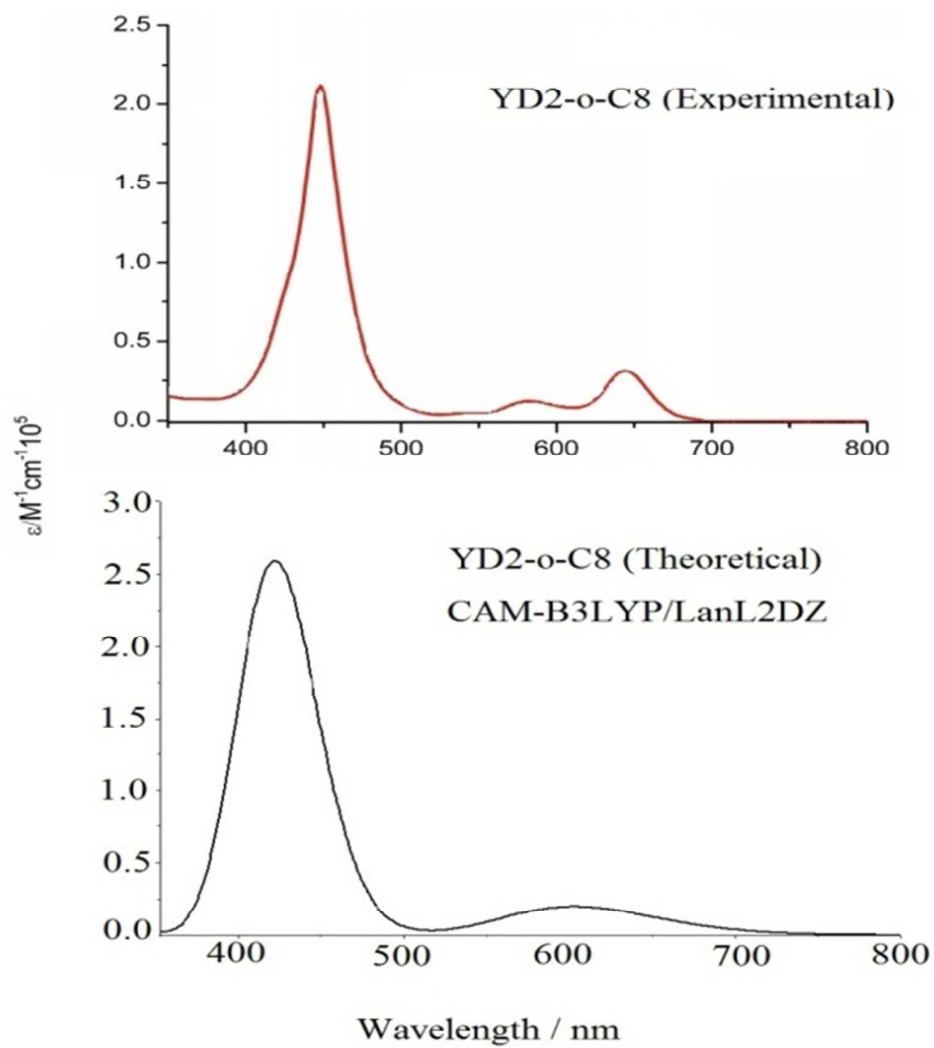


**Figure 2.** Comparison of experimental and calculated absorption spectrum of YD2-o-C8 dye in THF solution.

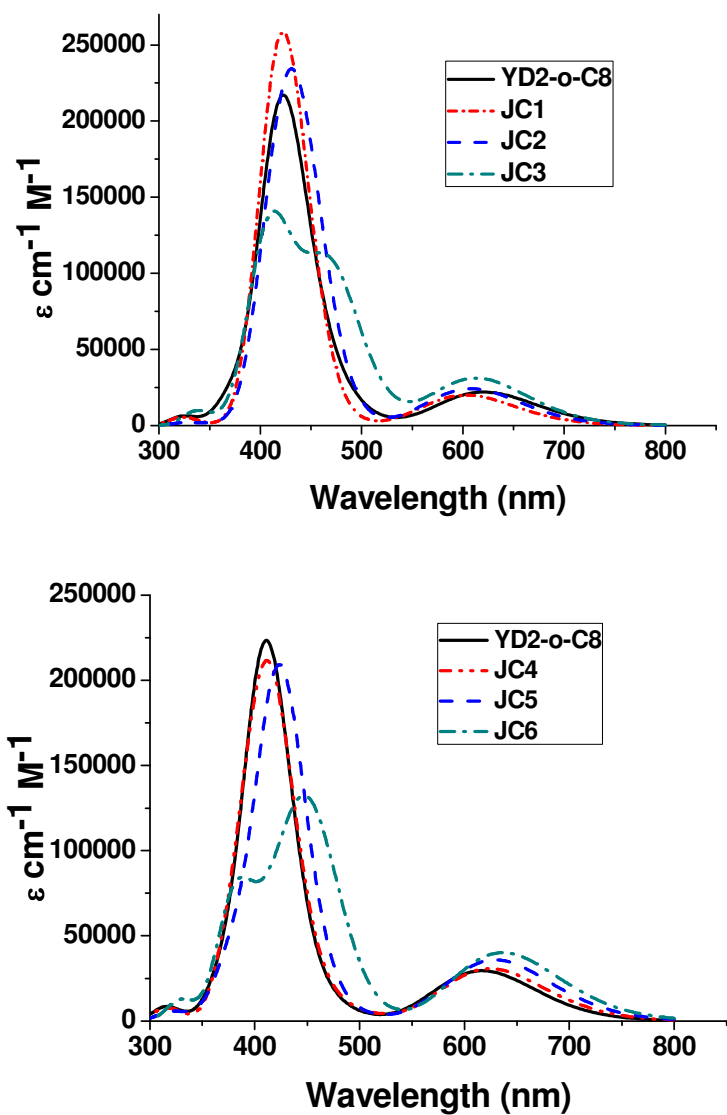


**Figure 3.** Calculated absorption spectra for the JC1 – 6 dyes in THF solution at the C-PCM – TDCAM – B3LYP/ LanL2DZ level of theory.

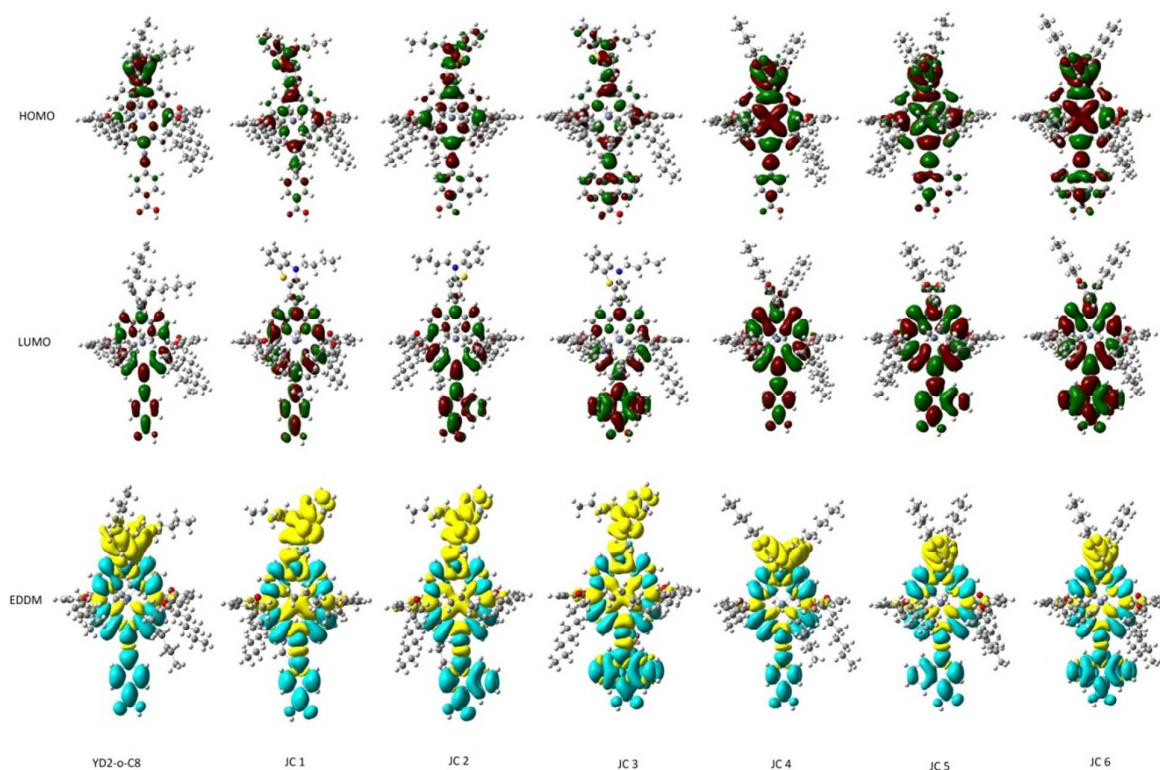


**Figure 4.** HOMO, LUMO, and electron density difference maps (EDDM) between the excited and ground states of JC1 – 6 and YD2-o-C8 dyes. The contour thresholds for molecular orbitals and density differences are 0.01 and 0.0001 a.u., respectively. The yellow and blue colors indicate a decrease and increase of charge densities, respectively.

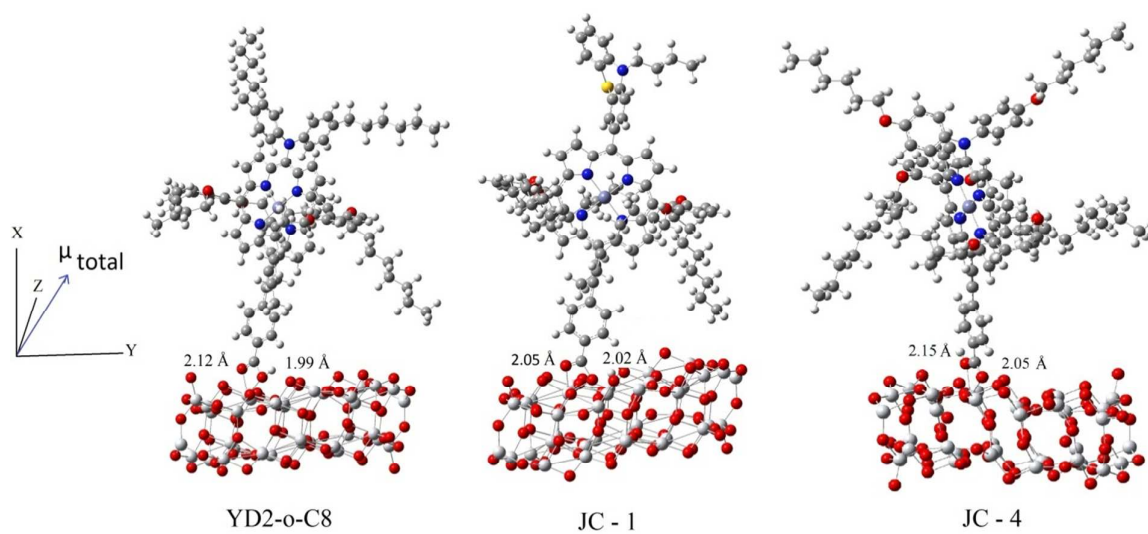


**Figure 5.** Optimized bidentate chelate bridging mode of YD2-o-C8, JC1 and JC4 dyes on the  $(\text{TiO}_2)_{36}$  cluster calculated by PBE/DNP on DMol3 program.

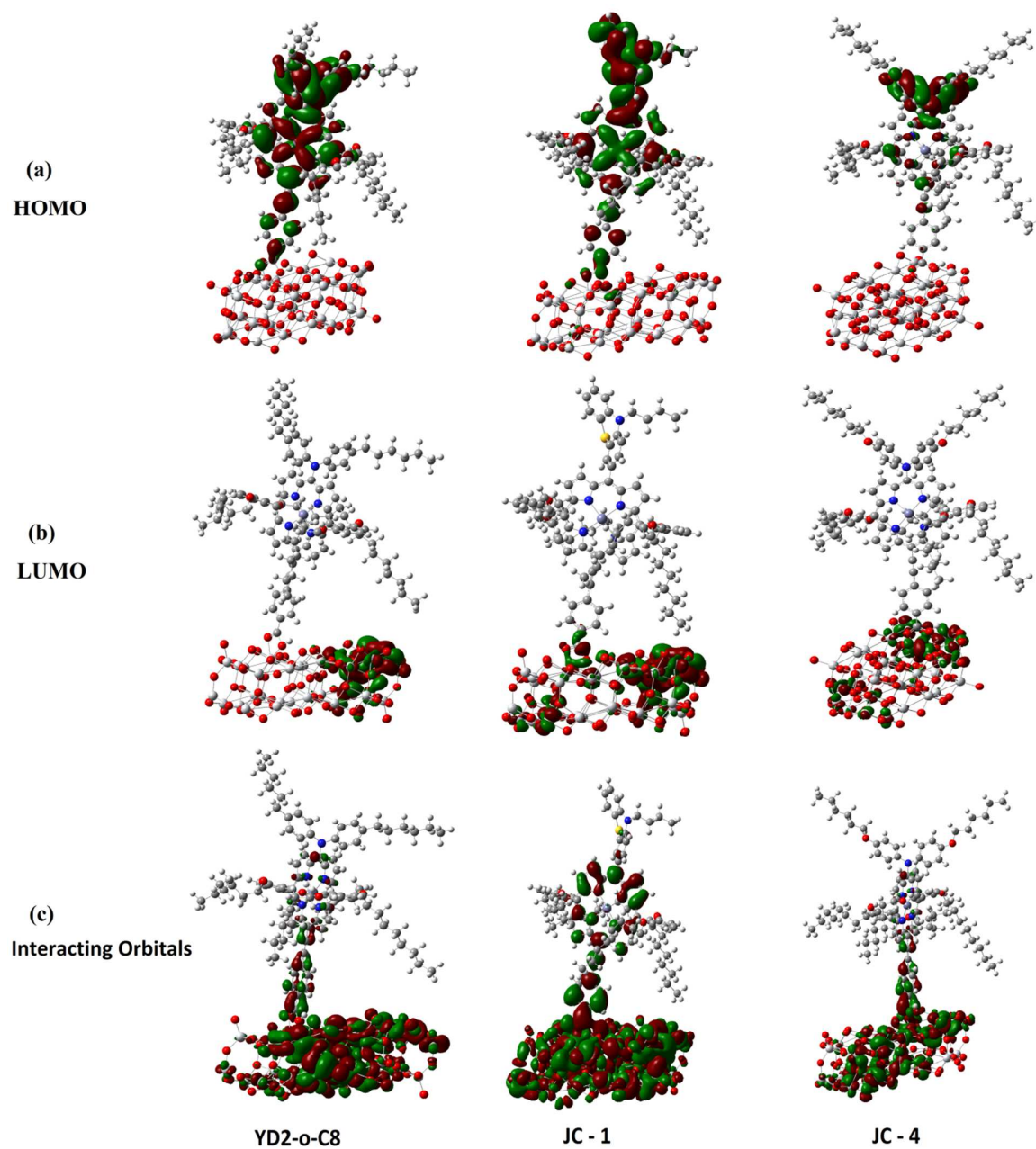
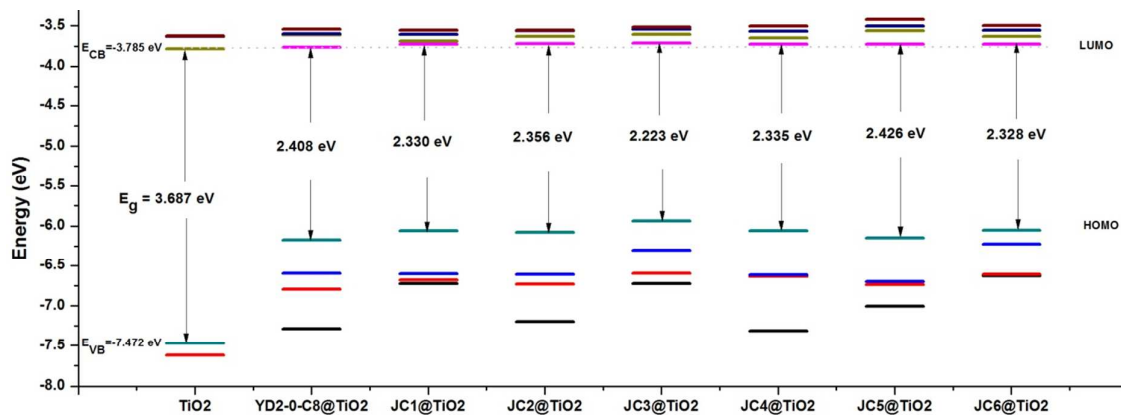


Figure 6. (a) HOMO (b) LUMO and (c) interacting orbital isosurfaces of reference dye YD2-o-C8 and JC1 dyes on the  $(\text{TiO}_2)_{36}$  nanoparticle. The isovalue is 0.001 a.u.



**Figure 7.** Energy level diagram of dye – TiO<sub>2</sub> systems investigated in the present study.